NANO LETTERS

Letter

pubs.acs.org/NanoLett

One-Step Synthesis of Hybrid Nanocrystals with Rational Tuning of the Morphology

Wei Sang, Tingting Zheng, Youcheng Wang, Xu Li, Xu Zhao, Jie Zeng,* and J. G. Hou

Hefei National Laboratory for Physical Sciences at the Microscale & Collaborative Innovation Center of Suzhou Nano Science and Technology, Center of Advanced Nanocatalysis (CAN-USTC) & Department of Chemical Physics, University of Science and Technology of China, Hefei, Anhui 230026, People's Republic of China

Supporting Information

ABSTRACT: Metal–sulfide hybrid nanocrystals (HNCs) have been of great interest for their distinguished interfacial effect, which gives rise to unique catalytic properties. However, most of the reported metal–sulfide HNCs were synthesized via two-step approaches and few were fabricated based on the one-step strategies. Herein, we report a facile one-pot synthesis of CuPt–Cu_2S, Pt–Cu_2S HNCs, and CuPt nanocubes by simply changing the Pt precursor types. 1-Hexadecanethiol (HDT) was employed in this system to mediate the reduction of metal precursors and also as capping agent and sulfur source. Moreover, CuPd–Cu_2S and Au–Cu_2S HNCs were successfully prepared by using this one-step method. The catalytic properties of the obtained three nanocrystals were investigated in hydrogenation of cinnamaldehyde. Results show that CuPt–Cu_2S HNCs exhibited the highest conversion rate and the highest selectivity toward hydrocinnamaldehyde while 3-phenyl-1-propanol was the only product over Pt–Cu_2S HNCs.

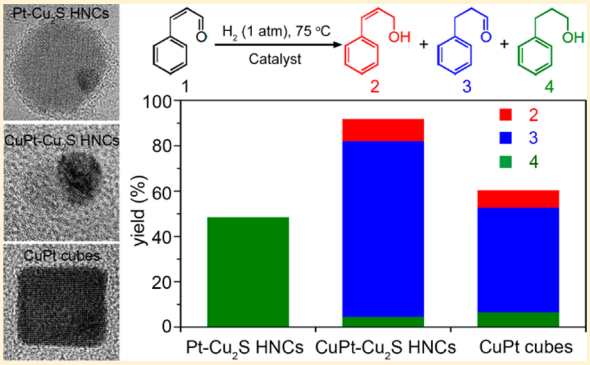

KEYWORDS: *one-step synthesis, metal–sulfide HNCs, structure control, hydrogenation of cinnamaldehyde, synergistic effect, interfacial function*

Platinum (Pt), a noble transition metal, possesses distinctive abilities in many important catalytic reactions such as partial oxidation, hydrogenation, and dehydrogenation.[1−5] In Pt-containing nanomaterials, Pt and different materials are integrated together at nanoscale to provide the system with tailored catalytic properties from the disparate component.[6,7] For example, by incorporating the 3d transition metal into Pt, PtM (M = Cu, Fe, Co, Ni, etc.) bimetallic nanocrystals (NCs) exhibit enhanced catalytic activity and durability due to the synergistic effect of two metals.[8−12] Enhancement of catalytic property can also be achieved by combining Pt with semiconductors. Pt-based metal–semiconductor hybrid nanocrystals (HNCs) consisting of both metal and semiconductor sections that are joined through direct contact are mostly distinguished by their interfacial effect.[13−17] In the case of metal–sulfide HNCs, specifically, charge transfer between metal and sulfide can modify the electronic structure and band alignment of both domains and thus may improve their catalytic properties.[18−20] For instance, electron flow from Ag_2S to Pt has been proved to improve the performance and stability in CO-stripping and methanol oxidation reaction.[21] However, investigation of metal–sulfide HNCs in organic catalysis still has been in a rudimentary state of development.[22]

Up to now, various well-defined morphologies of PtM alloy nanocrystals such as PtNi octahedron NCs, PtFe nanocubes, and PtCu dodecahedron NCs have been synthesized via the strategies of coreduction, thermal decomposition, galvanic replacement reaction, and so forth.[23−30] Such successes provide an effective platform for the development of immature synthesis of metal–sulfide HNCs. Metal–sulfide HNCs are mainly fabricated by two-step approaches in a wet chemical synthetic route. Seeded growth is the most commonly used strategy, in which metals deposit on the sulfide seeds or metal sulfides grow in situ on the metal seeds. Ru–Cu_2S, Pt–CdS, Ag–Ag_2S, Au@PbS HNCs, and so forth have been successfully prepared via seeded growth.[18,30−35] Recently, a sulfurization reaction has also been adopted in the synthesis of metal–sulfide HNCs. The added sulfur precursors such as inorganic sulfide (Na_2S, Na_2S_x, H_2S, etc.), sulfur powder, or organic sulfide (alkylthiol, metal thiobenzoate, etc.) can selectively sulfurize the as-prepared metal NCs, giving rise to the metal–sulfide HNCs with finely tuned architectures.[36−39] Despite these successes, the synthetic procedures involved in these two-step approaches are generally complex and time-consuming. One-step synthesis, a relatively simple and direct strategy which has been practiced more commonly in fabricating metal NCs, was also explored in the synthesis of metal–sulfide HNCs. However, few cases were reported due to the difficulty of controlling the reduction of

Received: August 31, 2014
Revised: October 9, 2014

dx.doi.org/10.1021/nl503343n | *Nano Lett.* XXXX, XXX, XXX–XXX

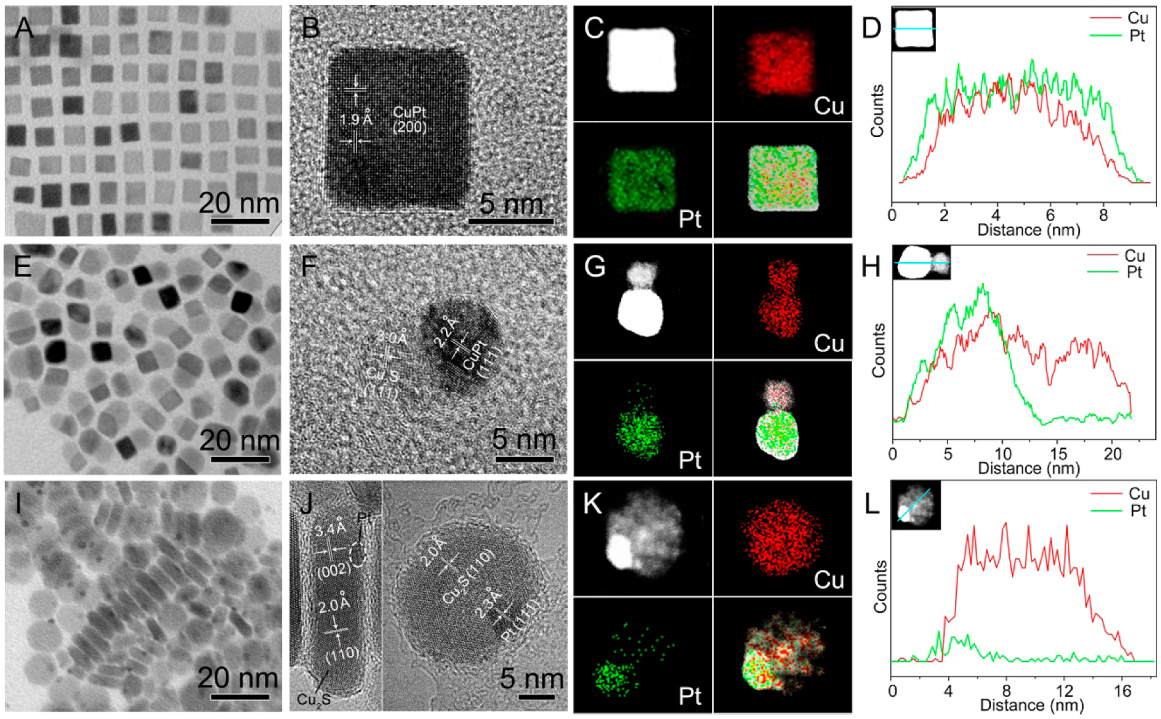

Figure 1. (A,E,I) TEM images of CuPt alloy nanocubes, CuPt–Cu_2S HNCs, and Pt–Cu_2S HNCs, respectively; (B,F,J) HRTEM images of CuPt alloy nanocubes, CuPt–Cu_2S HNCs, and Pt–Cu_2S HNCs, respectively; (C,G,K) HAADF-STEM images of CuPt alloy nanocubes, CuPt–Cu_2S HNCs, and Pt–Cu_2S HNCs, respectively, corresponding element maps showing the distribution of Pt (green) and Cu (red); (D,H,L) line scan profiles recorded from an individual CuPt alloy nanocubes, CuPt–Cu_2S HNCs, and Pt–Cu_2S HNCs, respectively.

metal precursors as well as sulfurization in the growth of metal–sulfide HNCs.

Herein, a newly developed one-step synthesis is demonstrated by our group to prepare CuPt–Cu_2S and Pt–Cu_2S HNCs, together with CuPt nanocubes by simply changing Pt precursor types with different reduction potentials. In the synthesis, 1-hexadecanethiol (HDT) acting as capping agent, ligand, and sulfur source was introduced to mediate the sequential reduction of metal precursors and sulfurization reaction. These three types of Pt-containing nanocrystals displayed different catalytic properties in the experiments of cinnamaldehyde hydrogenation, which was probably attributed to the synergistic function of two metals and the interfacial effect between metal and sulfide. This one-step system provided us with avenues to study the formation mechanism involved in the growth of metal–sulfide HNCs, which could in turn be further exploited to create more intricate Pt-based hybrid nanostructures.

The synthesis involves $Cu(acac)_2$ as Cu precursor, K_2PtCl_4, H_2PtCl_6, or $Pt(acac)_2$ as Pt precursors, and a mixture of 1-octadecene (ODE) and oleylamine (OAm) as solvent in which OAm also acts as reductant. Specifically, K_2PtCl_4, $Cu(acac)_2$, and HDT were added into a mixture of ODE and OAm. The solution was heated at 80 °C under magnetic stirring for 30 min to prepare a homogeneous mixture of reactants. It was then heated to 200 °C and maintained at this temperature for 2 h (see Experimental Section in Supporting Information for details). A representative transmission electron microscopy (TEM) image shows that the final products consist of CuPt nanocubes with an edge length of 8.0 ± 1.5 nm, which are uniform in shape (Figure 1A). An individual nanocube was further characterized by high-resolution transmission electron microscopy (HRTEM), where the lattice spacing of (200) plane matched well with that of the CuPt alloy (Figure 1B). Figure 1C presents the high-angle annular dark-field scanning TEM (HAADF-STEM) image of a typical nanocube, on which energy-dispersive X-ray (EDX) analysis was induced (Figure 1C and D). The EDX elemental mapping images and line-scanning profile demonstrate the complete overlapping of two metal components, indicating Cu and Pt are well alloyed throughout the whole nanocubes. To further reveal the crystalline structure of the nanocubes, powder X-ray diffraction (XRD) pattern is provided in Figure 2, which reveals a face-centered cubic (*fcc*) structure with the peak positions amid those of pure *fcc* Cu (JCPDS no. 85–1326) and pure *fcc* Pt (JCPDS no. 04–0802). Supporting Information Figure S1 shows the EDX spectrum that suggests that the atomic ratio of Cu and Pt was 2.1, agreeing well with the ratio obtained by inductively coupled plasma atomic emission spectroscopy (ICP-AES).

When the Pt precursor was switched to H_2PtCl_6 or $Pt(acac)_2$ with other conditions identical with those of the synthesis of CuPt nanocubes, CuPt–Cu_2S HNCs and Pt–Cu_2S HNCs were generated, respectively. A typical TEM image of CuPt–Cu_2S HNCs exhibits that the heterodimers in which the two domains show a clear color contrast, were produced in high yield and purity (Figure 1E). Figure 1F shows the representative HRTEM image of a single heterodimer. The two sets of lattice spacing marked on the dark domain and bright domain of a heterodimer, which are 2.2 and 3.0 Å, can be accredited to the (111) plane of CuPt and the (111) plane of Cu_2S, respectively. However, no obvious Cu_2S peaks were detected in the XRD pattern (Figure 2), indicating the poor crystallinity of Cu_2S domain.[40] In addition, the elemental distributions of Cu and Pt are revealed by the EDX elemental mapping, together with line-scanning on an individual CuPt–Cu_2S. As shown in Figure 1G,

dx.doi.org/10.1021/nl503343n | *Nano Lett.* XXXX, XXX, XXX–XXX

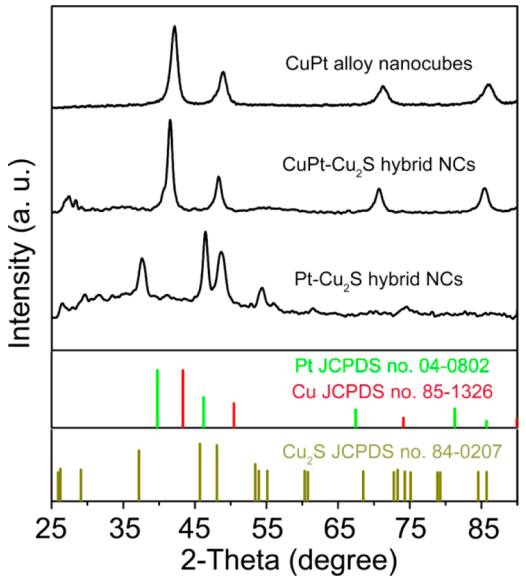

Figure 2. XRD patterns of CuPt alloy nanocubes, CuPt−Cu_2S HNCs, and Pt−Cu_2S HNCs, respectively.

the Cu element distributes throughout both domains of a heterodimer, whereas the Pt element scatters around only one domain, which was further backed by Figure 1H, unambiguously revealing the CuPt−Cu_2S heterodimer structure. A colloid of another hybrid nanocrystals, Pt−Cu_2S, was also resolved by TEM image in which both horizontally aligned and vertically stacked Pt−Cu_2S HNCs can be observed. The contour of the hybrid nanocrystal seems like a small particle growing on a circular nanoplate with an average diameter of 18.5 ± 6.4 nm and average thickness of 4.2 ± 1.2 nm (Figure 1I). As shown in the HRTEM images, the lattice fringe spacing of 2.3 Å marked on the small particle can be indexed to the (111) plane of Pt. The other two lattice fringes marked on the nanoplate with the same spacing of 2.0 Å taken from two angles both correspond to the (220) planes of Cu_2S nanoplate (Figure 1J). The (002) lattice fringe of Cu_2S can also be visible along the long axis of the hybrid nanocrystal on the left subimage of Figure 1J. Moreover, the EDX elemental mapping clearly shows a color difference between the circular area (mainly Cu, red) and the much smaller area (mainly Pt, green), confirming a hybrid nanostructure. The corresponding line-scanning profile recorded along the symmetric axis further supports the homogeneous distribution of Cu with Pt partially overlapped on its one end (Figure 1L). Different from the obtained CuPt−Cu_2S HNCs, the Cu_2S peak in the XRD pattern of Pt−Cu_2S HNCs was clearly distinguished (Figure 2), revealing the relatively high crystallinity of Cu_2S domains in Pt−Cu_2S HNCs. Therefore, the structure of the Pt−Cu_2S HNCs is evidently settled that a small Pt particle situates on the periphery of a Cu_2S circular nanoplate. To better substantiate the elemental valence state of CuPt−Cu_2S and Pt−Cu_2S HNCs, the X-ray photoelectron spectroscopy (XPS) was carried out. The Cu $2p_{1/2}$ and Cu $2p_{3/2}$ peaks were located at 952.5 and 932.5 eV, respectively, with no appearance of the satellite peaks (Supporting Information Figure S2E and H), which excluded the existence of Cu(II). The peaks at 917.4 and 919.7 eV, which correspond to Cu_2S and Cu(0), respectively, in the L3M45M45 Auger electro spectra of Cu (Supporting Information Figure S2F and I), furnish compelling evidence for the composition of the two HNCs. In addition, the Cu/Pt atomic ratios of CuPt−Cu_2S NCs and Pt−Cu_2S NCs determined by EDX spectrum match well with the result of ICP-AES, which were 1.5 and 9.3, respectively (Supporting Information Figure S1B and C).

To better understand the formation mechanism of the obtained three nanostructures, we monitored their growth process by taking TEM images of samples prepared at different reaction time points (Supporting Information Figure S3). The changes of Cu/Pt ratio as a function of reaction time were also plotted to facilitate an in-depth elucidation, which were determined by ICP-AES in the three types of products respectively (Figure 3). During the growth of CuPt nanocubes,

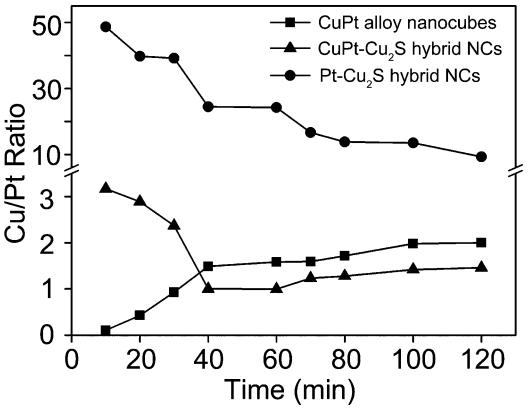

Figure 3. Plots of changes of Cu/Pt ratio in the three types of products as a function of reaction time. The ratio was determined by ICP-AES.

irregular nanocrystals with almost no Cu content were obtained at 10 min, and the Cu/Pt ratio of nanocrystals rapidly increased after that (Supporting Information Figure S3A and Figure 3). Based on the phenomena, one can deduce that irregular Pt-rich nuclei were first formed at the initial stage of growth. The subsequent codeposition of Pt and Cu led to the formation of CuPt nanocrystals with irregular shape. When the reaction was prolonged to 40 min, the CuPt nanocrystals evolved into cubic shape and coexisted with bits of small clusters (Supporting Information Figure S3B). In the meantime, Cu/Pt ratio increased to approximately 1.4 (Figure 3). More uniform nanocubes were observed at the later stage, presumably by Ostwald ripening (Supporting Information Figure S3C). In depth, we observed that CuPt alloy nanocrystals with irregular shape rather than cubic shape were obtained in the absence of HDT (Supporting Information Figure S5A), suggesting that the capping effect of HDT on CuPt (100) facets was responsible for the formation of CuPt nanocubes.

Supporting Information Figure S3D−F, illustrates the growth process of CuPt−Cu_2S HNCs. At the beginning 10 min of reaction, a large quantity of small nanocrystals with relatively high Cu/Pt ratio (above 3.3) were formed and the apparent decrease in Cu/Pt ratio of nanocrystals was detected as the growth proceeded (Figure 3 and Supporting Information Figure S3D). Therefore, one can speculate that CuPt nanocrystals were generated at the initial stage of growth with $Cu(acac)_2$ reduced much faster than Pt precursor, which is different from that in the formation of CuPt nanocubes. Considering the decreased Cu/Pt ratio and the later observation that no product was generated in the absence of Cu precursor (Supporting Information Figure S4E), we

dx.doi.org/10.1021/nl503343n | Nano Lett. XXXX, XXX, XXX−XXX

speculate that the galvanic replacement reaction (GRR) took place, in which initially formed Cu tiny crystals served as sacrificial templates and reacted with H_2PtCl_6 to generate CuPt nanocrystals. To verify this conjecture, we took the initially formed nanocrystals at the beginning 10 min of reaction and purified them with *n*-hexane. After centrifugation, these small nanocrystals were redispersed in the same growing solution without the addition of OAm as reducing agent and with the other conditions kept the same. Results show that these nanocrystals apparently grew larger (Supporting Information Figure S6) with the Cu/Pt ratio decreased from 3.3 to 1.7. The fact that nanocrystals can still grow in the absence of OAm provides a strong evidence for the involvement of GRR. After 40 min of reaction, the nanocrystals grew larger and some heterodimers with a bright small domain growing on one facet of CuPt nanocrystal were also observed (Supporting Information Figure S3E). Such initial formation of heterodimer well implicates that Cu_2S domain was beginning to generate, which was most likely induced by the sulfurization of Cu with HDT.[19,40] Further extension to 100 min resulted in the enlarged Cu_2S domains of similar size to CuPt domains (Supporting Information Figure S3F), suggesting that the later growth was mainly driven by the persisted sulfurization process, well in accordance with the increased Cu/Pt ratio (Figure 3). Interestingly, CuPt nanocages with a hollow structure were observed in the absence of HDT (Supporting Information Figure S5D), probably due to the enhanced GRR under no stabilization of the ligand. A similar nanocage was also reported recently by Xia et al., who demonstrated that the GRR was involved in the formation of CuPt nanocage.[9] By contrast, when the amount of HDT was increased to 45 μL, a few HNCs emerged and an excess amount of HDT (135 μL) gave rise to a great many uniform HNCs, which demonstrates the vital role of HDT played in the sulfurization reaction.

The growth of Pt−Cu_2S HNCs took a different path from that of the others. As shown in Figure 3 and Supporting Information Figure S3G, a large quantity of small HNCs with a quite high Cu/Pt ratio (approximates to 50) were obtained after 10 min of reaction. Considering the scarce Pt content in the initially formed HNCs, one can deduce that different from K_2PtCl_4, the reduction of $Pt(acac)_2$ was delayed. A plausible assumption is that the easier coordinating HDT with $Pt(acac)_2$ promoted the generation of Pt(II)-complex and lowered the reduction potential of $Pt(acac)_2$. To elucidate the existence of coordination, Fourier transform infrared (FT-IR) spectroscopy (Supporting Information Figure S7) was used to characterize $Pt(acac)_2$, HDT and the Pt(II)-HDT complex. Compared to the spectrum of $Pt(acac)_2$, the principal peaks of $Pt(acac)_2$ disappear in the spectrum of Pt(II)-HDT complex, demonstrating that ligand exchange occurred between $Pt(acac)_2$ and HDT. Besides, in the spectrum of HDT, the weak peak around 2600 cm^{-1} is assigned to −SH stretching vibration, which also vanishes in the spectrum of Pt(II)-HDT. In the subsequent growth stage, the apparently increasing size can be detected obviously in both domains, suggesting the further growth of both Cu_2S and Pt particles (Supporting Information Figure S3, H−I). In addition, we observed that no addition of HDT led to the generation of irregular CuPt alloy nanocrytals, whereas increasing the amount of HDT hindered the formation of Pt but favored the formation of Cu_2S domain (Supporting Information Figure S5G−I). Such observation confirms the essential role of HDT as sulfur source and also coincides with the above assumption that HDT acts as ligands that slow down the reduction of Pt^{II}.[41]

Our further experiments demonstrated that this one-pot strategy could be readily extended to the synthesis of CuPd−Cu_2S HNCs and Au−Cu_2S HNCs by simply changing the Pt precursor to Na_2PdCl_4 or $HAuCl_4$ while maintaining the other conditions. Typical TEM images of CuPd−Cu_2S HNCs (Supporting Information Figure S8A) and Au−Cu_2S HNCs (Supporting Information Figure S8D) displayed two side-by-side structures similar to Pt−Cu_2S HNCs. The corresponding line-scanning profiles recorded along the symmetric axis of the two nanocrystals show that CuPd or Au small nanocrystal is situated on the periphery of a large Cu_2S domain (Supporting Information Figure S8B and E). In the XRD patterns, Cu_2S and CuPd or Au peaks can be obviously discerned (Supporting Information Figure S8C and F). These results show that our method can be a general method to synthesize metal−sulfide HNCs and even more complicated hybrid nanostructures.

Catalytic properties of the obtained three nanocrystals were evaluated by the cinnamaldehyde hydrogenation reaction. Selective hydrogenation of α,β-unsaturated aldehydes such as cinnamaldehyde is an organic transformation of fundamental and industrial importance.[42] During the reaction, the hydrogenation of carbonyl (C═O) group leads to cinnamyl alcohol, that of the olefinic (C═C) group yields hydrocinnamaldehyde, and hydrogenation of the both groups produces 3-phenyl-1-propanol. The hydrogenation products of cinnamaldehyde are widely used in pharmaceuticals and perfumes. For example, hydrocinnamaldehyde was also used as an important intermediate in the preparation of a drug used in the treatment of HIV.[43] As shown in Figure 4A, the conversion of cinnamaldehyde after 15 h was in the order of CuPt−Cu_2S (100%) > CuPt (73.2%) > Pt−Cu_2S (60.9%). It was found that both on the CuPt nanocubes and CuPt−Cu_2S HNCs, the main product of reaction was hydrocinnamaldehyde with a yield of 55% and 86.4%, respectively, and little cinnamyl alcohol or 3-

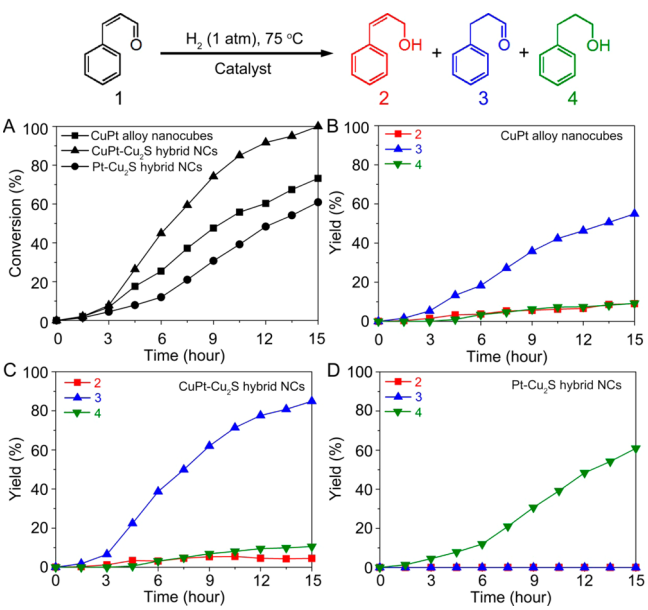

Figure 4. (A) Conversion of the reaction catalyzed by the three catalysts; time course of the reduction of cinnamaldehyde with H_2 using (B) CuPt alloy nanocubes, (C) CuPt−Cu_2S hybrid NCs, (D) Pt−Cu_2S hybrid NCs as catalysts.

dx.doi.org/10.1021/nl503343n | *Nano Lett.* XXXX, XXX, XXX−XXX

phenyl-1-propanol were produced. On the Pt−Cu_2S HNCs, however, 3-phenyl-1-propanol was the only product (Figure 4B−D). Considering the fact that Pt is the main active component and chemoselective for the reduction of carbonyl group, the electronic structure of Pt probably affected the selectivity of Pt−Cu_2S HNCs. As shown in the XPS data (Supporting Information Figure S2), the Pt $4f_{7/2}$ peak and $4f_{5/2}$ peak in the CuPt NCs and CuPt−Cu_2S HNCs were both observed at 70.9 and 74.2 eV, respectively. However, the corresponding two peaks for Pt−Cu_2S HNCs were both shifted to a higher level (71.6 and 74.9 eV, respectively). This result indicates that more electrons were transferred to Cu_2S from Pt, which probably induced the hydrogenation of olefinic group, and thus favored the generation of 3-phenyl-1-propanol.[44] Besides electron transfer, the steric effect of the small Pt nanocrystals might be also responsible for the formation of 3-phenyl-1-propanol.[45] Different from Pt−Cu_2S HNCs, both CuPt nanocubes and CuPt−Cu_2S HNCs possess the synergistic function of Cu and Pt, which might be the leading cause for the selective hydrogenation of olefinic group. Moreover, the higher selectivity of CuPt−Cu_2S HNCs toward hydrocinnamaldehyde than that of CuPt NCs was probably the result of the interfacial effect induced by the integration of Cu_2S domain.[6,22] Previous studies showed that the strong electron coupling in the form of electron transfer from metals to semiconductors could reduce the electron density in metal domains, which would favor the adsorption of C=C on the surface of metals and, thus, the generation of hydrocinnamaldehyde.

In summary, CuPt nanocubes, CuPt−Cu_2S HNCs, and Pt−Cu_2S HNCs were prepared respectively in a facile one-step synthesis. By changing Pt precursor types and taking advantage of the different coordination abilities of HDT toward different Pt precursors, the reduction potential of Pt ions can be mediated and the reduction sequences of two metal precursors can be thus well controlled. Additionally, HDT served as capping agent in the growth of CuPt nanocubes and also as the sulfur source in the sulfurization reaction to form Pt−Cu_2S and CuPt−Cu_2S HNCs. Furthermore, CuPd−Cu_2S and Au−Cu_2S HNCs were successfully prepared by using this one-step method. In the experiment of cinnamaldehyde hydrogenation, Pt−Cu_2S HNCs simultaneously hydrogenated both the olefinic and carbonyl groups. The other two CuPt-containing NCs that are endowed with the synergistic function of Cu and Pt were chemoselective for the reduction of olefinic group. Besides, the higher selectivity of CuPt−Cu_2S HNCs toward hydrocinnamaldehyde relative to CuPt NCs was probably attributed to the interfacial effect. We believe that the rational design and synthesis of Pt-containing nanomaterials will provide the tool box for future endeavors in the fabrication of functional complex nanostructures.

■ ASSOCIATED CONTENT

Ⓢ Supporting Information

Experimental details, EDX spectra and XPS spectra of the three Pt-based nanocrystals, TEM images of samples obtained at different time points, TEM images of products prepared using different amounts of precursors, TEM images of nanocrystals obtained with different amounts of HDT, TEM images showing the GRR process, FT-IR spectra of $Pt(acac)_2$, HDT, and Pt(II)−HDT complex, and the characterization of CuPd−Cu_2S and Au−Cu_2S HNCs. This material is available free of charge via the Internet at http://pubs.acs.org.

■ AUTHOR INFORMATION

Corresponding Author

*E-mail: zengj@ustc.edu.cn.

Author Contributions

The manuscript was written through contributions of all authors. All authors have given approval to the final version of the manuscript.

Notes

The authors declare no competing financial interest.

■ ACKNOWLEDGMENTS

This work was supported by MOST of China (2014CB932700 and 2011CB921403), NSFC under Grant Nos. 21203173, 51371164, and J1030412, Strategic Priority Research Program B of the CAS under Grant No. XDB01020000, and Fundamental Research Funds for the Central Universities (WK2340000050 and WK2060190025).

■ REFERENCES

(1) Ertl, G.; Knözinger, H.; Schüth, F.; Weitkamp, J. *Handbook of Heterogeneous Catalysis*, 2nd ed.; Wiley-VCH: Weinheim, 2008, 247−262.
(2) Peng, Z.; Yang, H. *Nano Today* **2009**, *4*, 143−164.
(3) Chen, J.; Lim, B.; Lee, E. P.; Xia, Y. *Nano Today* **2009**, *4*, 81−95.
(4) An, K.; Alayoglu, S.; Musselwhite, N.; Na, K.; Somorjai, G. A. *J. Am. Chem. Soc.* **2014**, *136*, 6830−6833.
(5) Habas, S. E.; Lee, H.; Radmilovic, V.; Somorjai, G. A.; Yang, P. *Nat. Mater.* **2007**, *6*, 692−697.
(6) Yu, W.; Porosoff, M. D.; Chen, J. G. *Chem. Rev.* **2012**, *112*, 5780−5817.
(7) Chen, H.; Wang, D.; Yu, Y.; Newton, K. A.; Muller, D. A.; Abruña, H.; DiSalvo, F. J. *J. Am. Chem. Soc.* **2012**, *134*, 18453−18459.
(8) Liu, Q.; Yan, Z.; Henderson, N. L.; Bauer, J. C.; Goodman, D. W.; Batteas, J. D.; Schaak, R. E. *J. Am. Chem. Soc.* **2009**, *131*, 5720−5721.
(9) Xia, B. Y.; Wu, H. B.; Wang, X.; Lou, X. W. *J. Am. Chem. Soc.* **2012**, *134*, 13934−13937.
(10) Wangm, G.-H.; Hilgert, J.; Richter, F. H.; Wang, F.; Bongard, H.-J.; Spliethoff, B.; Weidenthaler, C.; Ferdi, S. *Nat. Mater.* **2014**, *13*, 293−300.
(11) Cui, C.; Gan, L.; Li, H.-H.; Yu, S.-H.; Heggen, M.; Strasser, P. *Nano Lett.* **2012**, *12*, 5885−5889.
(12) Chen, C.; Kang, Y.; Huo, Z.; Zhu, Z.; Huang, W.; Xin, H. L.; Snyder, J. D.; Li, D.; Herron, J. A.; Mavrikakis, M.; Chi, M.; More, K. L.; Li, Y.; Markovic, N. M.; Somorjai, G. A.; Yang, P.; Stamenkovic, V. R. *Science* **2014**, *323*, 1339−1343.
(13) George, C.; Dorfs, D.; Bertoni, G.; Falqui, A.; Genovese, A.; Pellegrino, T.; Roig, A.; Quarta, A.; Comparelli, R.; Curri, M. L.; Cingolani, R.; Manna, L. *J. Am. Chem. Soc.* **2011**, *133*, 2205−2217.
(14) Habas, S. E.; Yang, P.; Mokari, T. *J. Am. Chem. Soc.* **2008**, *130*, 3294−3295.
(15) Buck, M. R.; Bondi, J. F.; Schaak, R. E. *Nat. Chem.* **2012**, *4*, 37−44.
(16) Hodges, J. M.; Biacchi, A. J.; Schaak, R. E. *ACS Nano* **2014**, *8*, 1047−1055.
(17) Cargnello, M.; Doan-Nguyen, V. V. T.; Gordon, T. R.; Diaz, R. E.; Stach, E. A.; Gorte, R. J.; Fornasiero, P.; Murray, C. B. *Science* **2013**, *341*, 771−773.
(18) Macdonald, J. E.; Sadan, M. B.; Houben, L.; Popov, I.; Banin, U. *Nat. Mater.* **2010**, *9*, 810−815.
(19) Zeng, J.; Huang, J.; Liu, C.; Wu, C. H.; Lin, Y.; Wang, X.; Zhang, S.; Hou, J.; Xia, Y. *Adv. Mater.* **2010**, *22*, 1936−1940.
(20) Chakrabortty, S.; Yang, J. A.; Tan, Y. M.; Mishra, N.; Chan, Y. *Angew. Chem., Int. Ed.* **2010**, *49*, 2888−2892.
(21) Yang, J.; Ying, J. Y. *Angew. Chem., Int. Ed.* **2011**, *50*, 4637−4643.

(22) Zhang, Z.-C.; Xu, B.; Wang, X. *Chem. Soc. Rev.* **2014**, DOI: 10.1039/C3CS60389J.
(23) Wang, D.; Li, Y. *Adv. Mater.* **2011**, *23*, 1044−1060.
(24) Jia, Y.; Jiang, Y.; Zhang, J.; Zhang, L.; Chen, Q.; Xie, Z.; Zheng, L. *J. Am. Chem. Soc.* **2014**, *136*, 3748−3751.
(25) Wu, J.; Zhang, J.; Peng, Z.; Yang, S.; Wagner, F. T.; Yang, H. *J. Am. Chem. Soc.* **2010**, *132*, 4984−4985.
(26) Chen, M.; Kim, J.; Liu, J. P.; Fan, H.; Sun, S. *J. Am. Chem. Soc.* **2006**, *128*, 7132−7133.
(27) Zhang, L.; Zhuang, J.; Kuang, Q.; Xie, S.; Jiang, Z.; Xie, Z.; Zheng, L. *J. Am. Chem. Soc.* **2011**, *133*, 17114−17117.
(28) Lu, Y.; Zhao, Y.; Yu, L.; Dong, L.; Shi, C.; Hu, M.-J.; Xu, Y.-J.; Wen, L.-P.; Yu, S.-H. *Adv. Mater.* **2010**, *22*, 1407−1411.
(29) Yu, Y.; Zhang, Q.; Xie, J.; Lee, J. Y. *Nat. Commun.* **2013**, *4*, 1454 DOI: 10.1038/ncomms2474.
(30) Liu, Y.; Walker, A. R. H. *ACS Nano* **2011**, *5*, 6843−6854.
(31) Costi, R.; Saunders, A. E.; Banin, U. *Angew. Chem., Int. Ed.* **2010**, *49*, 2−22.
(32) Lee, J.-S.; Shevchenko, E. V.; Talapin, D. V. *J. Am. Chem. Soc.* **2008**, *130*, 9673−9675.
(33) Zeng, J.; Tao, J.; Su, D.; Zhu, Y.; Qin, D.; Xia, Y. *Nano Lett.* **2011**, *11*, 3010−3015.
(34) Lamgbright, S.; Butaeva, E.; Razgoniaeva, N.; Hopkins, T.; Smith, B.; Perera, D.; Corbin, J.; Khon, E.; Thomas, R.; Moroz, P.; Mereshchenko, A.; Tarnovsky, A.; Zamkov, M. *ACS Nano* **2014**, *8*, 352−361.
(35) Fan, F.-R.; Ding, Y.; Liu, D.-Y.; Tian, Z.-Q.; Wang, Z.-L. *J. Am. Chem. Soc.* **2009**, *131*, 12036−12037.
(36) Liu, Y.; Walker, A. R. H. *J. Phys. Chem. C* **2010**, *114*, 4264−4271.
(37) Sun, Z.; Yang, Z.; Zhou, J.; Yeung, M. H.; Ni, W.; Wu, H.; Wang, J. *Angew. Chem., Int. Ed.* **2009**, *48*, 2881−2885.
(38) Lee, S.-U.; Hong, J. W.; Choi, S.-I; Han, S. W. *J. Am. Chem. Soc.* **2014**, *136*, 5221−5224.
(39) Hsu, S.-W.; Ngo, C.; Tao, A. R. *Nano Lett.* **2014**, *14*, 2372−2380.
(40) Ding, X.; Zou, Y.; Jiang, J. *J. Mater. Chem.* **2012**, *22*, 23169−23174.
(41) Liu, Y.; Walker, A. R. H. *Angew. Chem., Int. Ed.* **2010**, *49*, 6781−6785.
(42) Loffreda, D.; Delbecq, F.; Vigné, F.; Sautet, P. *Angew. Chem., Int. Ed.* **2005**, *44*, 5279−5282.
(43) Mäki-Arvela, P.; Hajek, J.; Salmi, T.; Murzin, D. Y. *Appl. Catal., A* **2005**, *292*, 1−49.
(44) Gallezot, P.; Richard, D. *Catal. Rev. Sci. Eng.* **1998**, *40*, 81−126.
(45) Giroir, F. A.; Richard, D.; Gallezot, P. *Catal. Lett.* **1990**, *5*, 175−181.